

Application of a Continuum Mean Field Approximation to Fullerenes in Lipid Bilayers

R.J.K. Udayana Ranatunga and Steven O. Nielsen*

Department of Chemistry, University of Texas at Dallas, 800 West Campbell Road, Richardson, TX 75080, USA

Abstract: Biological applications of fullerenes are severely impeded by our incomplete understanding of their toxicity. Here we extend a recently developed computational method to gain insight into the behavior of fullerenes in lipid bilayer systems. The physical behavior of fullerenes is captured through a continuum model incorporating both their hollow geometry and surface chemistry. By using this model in molecular dynamics simulations we are able to continuously vary the fullerene size and study the resulting variation in equilibrium position, solvation free energy and water to lipid transfer free energy. The results show agreement with all-atom and coarse grained fullerene models and can be extended to study the aggregation of fullerenes in lipid bilayers.

Keywords: Fullerenes, lipid bilayer, solvation free energy, nanoparticles, bio-nano interactions, mean field model, molecular dynamics, coarse grain, transfer free energy, Hamaker summation.

1. INTRODUCTION

Hand in hand with the integration of nanomaterials into current technology comes the elevated possibility of nanomaterial exposure to living organisms, either explicitly through biomedical application or indirectly through environmental contamination [1,2]. It is clear that to further develop and utilize nanomaterials safely, a strategy involving both experimentation on specific nanomaterial systems, and theoretical investigations on classes of nanomaterials is necessary. In this study we focus on a specific class of nanomaterials, fullerenes, with an emphasis on the behavior of these particles in lipid membranes.

Fullerenes are discrete graphitic carbon based molecules which possess a closed-cage structure. From these, examples of fullerenes with sphere-like geometries include C_{20} , C_{28} , C_{60} (Buckminster fullerene), C_{80} , C_{180} , C_{240} , C_{320} and C_{540} which range from 2.0 to 10.5 Å in radius. The special physical, chemical and optoelectronic properties of these graphitic particles make them candidates for application in fields such as organic photovoltaics [3], optoelectronic devices [4], cell imaging [5] and drug delivery [6].

The interest in applications of fullerenes is tempered by concerns over their toxicity. Unfortunately, the diversity of the potential applications of these molecules opens possibilities for human exposure through inhalation, dermal and oral routes [7] as well as from intravenous delivery in the case of biomedical application [8]. The range of entry routes require toxicity studies to examine biological responses at several possible exposure sites as well as distal sites where fullerenes may be concentrated through physiological processes [8]. *In vivo* studies pertaining to fullerenes and fullerene derivatives have in general shown that a majority of those absorbed remain at the site of exposure, although accumulation in the liver, kidneys, spleen and metabolism and elimination are also observed [8,9]. On the other hand, *in vitro* studies have focused on dermal [8,10] and cardiovascular models [8,11] and have studied the mechanisms which result in fullerene toxicity. In studying the cellular uptake of fullerenes, their entry and aggregation in cell membranes is particularly important.

Apart from experimental studies, computer simulation techniques have been utilized to elucidate the passive diffusion of C_{60} and C_{60} aggregates into model membranes [12-17]. Such studies

have the advantage of high spatial and temporal resolution in addition to precise control of system composition and conditions. Although the simulation of complete biological systems is still beyond the capabilities of conventional computer modeling, studies of fullerenes in lipid bilayers may yield valuable insight into the mechanisms leading to toxicity and strategies to mitigate their toxic effect. For example, the aggregation tendency with particle size and the strength of associative interactions of fullerenes in a membrane may provide insight to experimentalists on the derivatization necessary to circumvent aggregation. This is particularly significant due to reported correlations between the aggregation behavior of fullerenes and toxicity [18].

In this study we present coarse grained (CG) molecular dynamics studies of fullerenes in dioleoylphosphatidylcholine (DOPC) lipid bilayer membranes employing a continuum mean field model for the fullerene. Mean field models approximate the effect of a many bodied system through single body potentials. These models have a long history in the literature. For example, the Hamaker summation method [19] assumes a solid with homogeneous interaction site density, and evaluates the net interaction energy of two such objects using integration. However, the Hamaker theory makes a low curvature assumption to evaluate the integral making the resulting energy expression unreliable at small interaction distances. The limitation arising from this curvature assumption was removed by Henderson among others [20]. Notably, Girifalco [21] used a mean field model of C_{60} to evaluate several gas and solid phase properties. By considering all-atom simulations, he suggests that at ambient temperatures the free rotation of C_{60} presents an effective potential to the environment which is inherently spherically averaged, thus providing justification for the mean field model.

We should note here that the mean field treatment is only applied to the fullerene particle. The lipids and solvent remain multi-body and the molecular dynamics simulations contain fluctuations and correlations between these molecules and the fullerene.

The article is organized as follows. In the Methods section we give details on the representation of the system components and our model of fullerenes. The free energy methods used are also discussed with a focus on the theory which allows for a straightforward calculation of solvation free energies. In the Results and Discussion section we begin by examining the hollow spherical geometry of fullerenes, and contrasting the interaction potentials arising from such a geometry with those arising from a filled sphere geometry. Next the solvation free energy of fullerenes in different

*Address correspondence to this author at the Department of Chemistry, University of Texas at Dallas, 800 West Campbell Road, Richardson, TX 75080, USA; Tel: 1-(972)-883-5323; Fax: 1-(972)-883-2925; E-mail: steven.nielsen@utdallas.edu

environments is computed leading to a discussion of the stability of fullerenes in a lipid membrane. Subsequently the variation of the lipid to water transfer free energy with fullerene size is evaluated which is an important factor influencing the phase partitioning behavior of the fullerenes. Finally, we conclude with an outlook of the modeling approach and discuss extending the methods introduced here to particle aggregates.

2. METHODS

Soft Component Interactions

To carry out molecular dynamics (MD) simulations a force field must be used which defines the representation of the system components and the interactions between them. To represent DOPC lipids and water the coarse grained force field of Shinoda *et al.* [22-24] was used while the fullerenes were represented using a continuum model.

The soft matter force field generally maps 3-4 heavy atoms to a single CG bead. The force field has been extensively parameterized against both experimental and all-atom simulation data and reproduces key thermodynamic quantities of liquid interfaces [23] and the phase behavior of lipids [24].

Dispersive interactions between soft matter beads i and j are treated through a Lennard-Jones potential, which takes the form

$$U(d_{ij}) = B\epsilon_{ij} \left\{ (\sigma_{ij}/d_{ij})^m - (\sigma_{ij}/d_{ij})^n \right\} \quad (1)$$

where d_{ij} is the separation distance, ϵ_{ij} is the interaction strength and σ_{ij} is a size parameter. The values of m and n are parameterization variables chosen to most suitably represent specific interactions and the prefactor B is chosen such that ϵ_{ij} is the well depth of this potential. Bond stretching is modeled using a harmonic potential, while bond bending is a superposition of a harmonic potential and a potential between 1-3 bonded pairs [24]. For further details on the soft matter force field we refer the reader to the primary references [22,24].

Fullerene Interactions

As an extension to our previous work [25,26] we employ a mean field continuum model for the fullerene. In this spirit, the fullerene is considered to be a hollow (as opposed to a filled) sphere with no discrete interaction sites but rather an interaction surface with a uniform site density of ρ_s . Using this model, the interaction of a fullerene particle p and a soft matter bead i can be evaluated using integration. For a particle of radius r at a distance R from an interaction site i (see Fig. 1), the net interaction U_{pi} is simply

$$U_{pi}(R; r) = \int_0^{2\pi} d\theta \int_0^\pi d\phi \rho_s r^2 \sin\phi U(d) \quad (2)$$

where d is the distance between i and the integration point on the fullerene, $d^2 = r^2 - 2rR\cos\phi + R^2$ (see Fig. 1), and $U(d)$ is the Lennard-Jones potential given in Eq. 1. This integral approach can be considered a mean field approximation, akin to the Hamaker summation method [19] for the interaction of two solid bodies. For $U(d)$ with parameters $m=9$, $n=6$, and $B=27/4$ the analytical expression U_{pi} is

$$U_{pi}(R; r) = 27\pi\rho_s\epsilon_{pi}r^2 \left(\frac{r^6 + 21r^4R^2 + 35r^2R^4 + 7R^6}{7R(R^2 - r^2)^7} \right) \sigma_{pi}^9 - 27\pi\rho_s\epsilon_{pi}r^2 \left(\frac{(r^2 + R^2)\sigma_{pi}^6}{(R^2 - r^2)^4} \right) \quad (3)$$

However, in practice $U(d)$ is truncated at 15.0 Å and hence the integral is numerically evaluated for use in MD simulations.

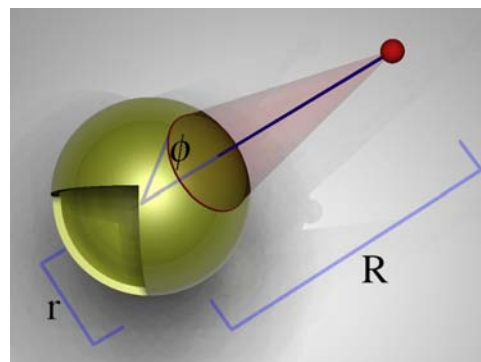


Fig. (1). The continuum mean field model of a fullerene particle. The interaction sites on the fullerene are smeared uniformly over the fullerene surface such that the net interaction between the particle and a soft matter bead can be found through integration (see Eq. 2).

Simulation Setup and Details

Simulation cells for the MD runs were populated with 200 dioleoylphosphatidylcholine (DOPC) lipid molecules in a bilayer parallel to the xy plane. The bilayers were solvated with CG water corresponding to 50 water molecules per lipid. Periodic boundary conditions were applied for all simulations. A representative snapshot of a simulation box is shown in Fig. (2).

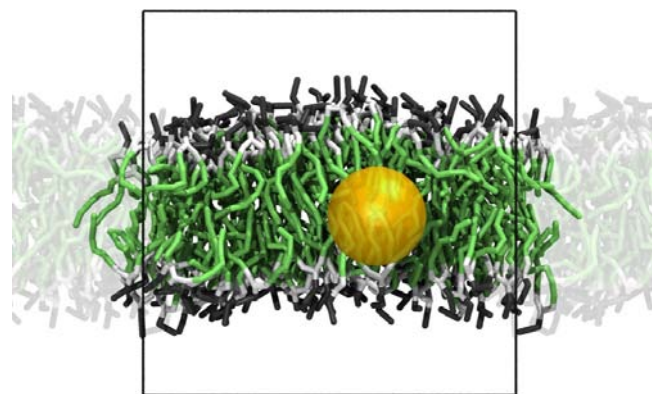


Fig. (2). A snapshot of a simulation cell showing a C_{540} molecule in a DOPC lipid bilayer. Water is not shown, and the C_{540} has been highlighted for clarity. The hydrophilic heads are black while the glycerol segment is white. The acyl chains are shaded in grey.

All simulations were carried out using the LAMMPS package developed by Sandia National Research Labs [27]. A Nosé-Hoover thermostat at 303 K and barostat at 1 atm was used to sample from the isothermal-isobaric ensemble [28]. Simulation cells were allowed to vary freely according to the applied pressure in the z direction while being constrained to undergo isotropic variations in the x,y directions. A multistep rRESPA [29] integrator was used in the propagation of the positions and the velocities of the beads. A long ranged interaction timestep of 20 fs was used while a timestep of 2 fs was used for short-ranged and bonded interactions.

Evaluation of Solvation Free Energy

The conventional definition of the excess solvation free energy of a particle is the free energy cost of transferring the particle from an ideal gas reference state into its solvated environment. Here we use a novel method we have developed for continuum particles [26]

where the solvation free energy of a particle with radius r is found through the relation

$$G_{\text{solv}}(r) = \int_0^r \frac{\partial G}{\partial \xi} d\xi \quad (4)$$

where G is the free energy of the system and ξ represents intermediate particle sizes between 0 and r . Statistical mechanics affirms that for the isothermal-isobaric ensemble

$$\frac{\partial G}{\partial r} = \frac{\partial}{\partial r} \left(\frac{1}{\beta} \ln \Delta \right) = \left\langle \sum_i \frac{\partial U_{pi}}{\partial r} \right\rangle + P \left\langle \frac{\partial V}{\partial r} \right\rangle \quad (5)$$

where Δ is the isothermal-isobaric partition function [30]. The left term in angle brackets is understood to be the ensemble averaged derivative of the interaction potential of the fullerene with all other beads in the system. The right term in angle brackets is negligibly small and in practice can be omitted.

The continuum mean field model gives ready access to $\langle \sum \partial U_{pi}(R;r) / \partial r \rangle$, by simply summing the individual $\partial U_{pi} / \partial r$ contributions (see Eq. 3) from interactions involving the fullerene and then averaging the sum over a MD trajectory.

The free energies for fullerene solvation in water and in a DOPC bilayer membrane were calculated. The radius values used were $r = 0.5, 0.7, 1.0, 1.2, 1.4, 1.6, 1.8, 2.0, 2.5, 3.0, 3.5, 4.0, 4.5, 5.0, 5.5, 6.0, 6.5, 7.0, 7.5, 8.0, 8.5, 9.0, 9.5, 10, \text{ and } 11 \text{ \AA}$. Systems were equilibrated for 10 ns prior to data collection runs of 20 ns. Apart from these particle radii, simulations were also run to correspond to the fullerenes C_{60} ($r=3.50 \text{ \AA}$), C_{80} ($r=4.11 \text{ \AA}$), C_{180} ($r=6.12 \text{ \AA}$), C_{240} ($r=7.12 \text{ \AA}$), C_{320} ($r=8.15 \text{ \AA}$) and C_{540} ($r=10.55 \text{ \AA}$). These simulations were equilibrated for 10 ns before data collection runs of 50 ns.

During these simulations the fullerenes are free of any externally imposed constraints and consequently show thermally driven motion. To study the positioning of the fullerene with respect to the lipid bilayer, the z distance of the fullerene from the center of mass of the lipid bilayer was collected during the simulations.

RESULTS AND DISCUSSION

The goal of this research is to understand the behavior of fullerenes in lipid membranes. Towards this end we use a continuum mean field model for the fullerene which allows us to evaluate the variation of physical properties with fullerene size. We begin by discussing our model of the fullerene, and in particular examine the role of the geometry of the fullerene on its interaction behavior.

Fullerene Model

The fullerene model used in this study is a hollow sphere with homogenous interaction site density over its surface of radius r . This is different from the actual atomic structure of a fullerene which has facets giving a spread of values for the distances of atoms from the center of mass (COM).

The net interaction potential of a liquid site i and the fullerene particle (U_{pi} , see Eq. 3) can be evaluated analytically or numerically as described in the Methods section. This results in a potential with a minimum $\sim 3.00 \text{ \AA}$ away from the surface of the particle, increasing sharply at distances closer to the surface (see Fig. 3). As the fullerene size increases the well depth is lowered while the energy minimum is shifted to larger values corresponding to the change in size. However, the well depth converges to a finite value, i.e. to that of a planar surface, at very large particle sizes.

In order to make the fullerene mean field approximation as realistic as possible, a suitable choice of the parameters is required. Recently, the CG force field we have used for the soft matter

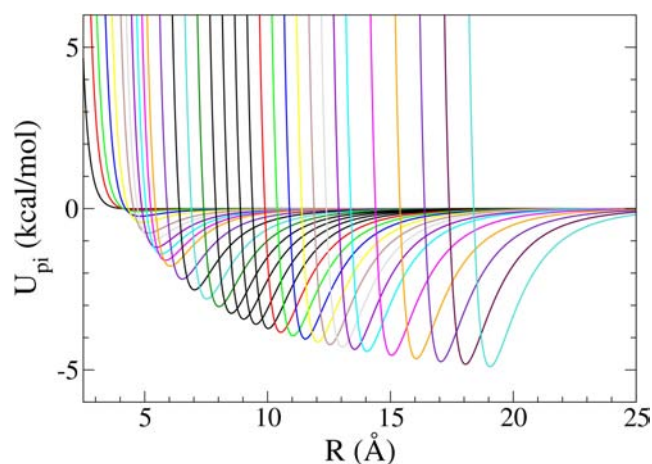


Fig. (3). The variation of the $U_{pi}(R;r)$ potential curves with particle radius r . The curves are plotted for particles sizes $r=0.1, 0.2, 0.3, 0.5, 0.7, 1.0, 1.2, 1.6, 1.8, 2.0, 2.5, 3.0, 3.5, \dots, 10, 11, 12, 13, 14, 15 \text{ \AA}$. The net interaction potential U_{pi} between a fullerene (p) and a soft component bead (i) shifts to larger separations and lower minima with r . The well depth converges at infinitely large particle sizes to that of a planar interface.

components has been extended to include aromatic compounds [31] and in particular fullerenes [32]. Due to the excellent compatibility of the graphitic carbon (BER bead) parameters with the soft components [14], the BER bead was used as the basis of the continuum model.

From Eqs. 2 and 3 it is clear that only a few parameters ($r, \rho_s, \epsilon_{pi}, \sigma_{pi}$) are required to specify the fullerene interactions. The $\epsilon_{pi}, \sigma_{pi}$ are taken from the published BER bead values [31], and the r for specific fullerenes (e.g. C_{60}, C_{180}) is calculated using the geometric mean of carbon atom positions relative to the fullerene COM in the all-atom representation. The surface site density ρ_s for fullerenes depends on the surface curvature; for example, ρ_s of C_{60} (0.3789 \AA^{-2}) is different from that of C_{540} (0.4000 \AA^{-2}). Because we wish to investigate the variation of properties due to one variable, namely the radius only, a fixed ρ_s value of 0.39 \AA^{-2} atomic sites per unit area is used.¹ These parameters result in potential curves for the implicit mean field model which are shown for C_{60} ($r = 3.50 \text{ \AA}$) and C_{540} ($r = 10.55 \text{ \AA}$) in Fig. (4). The plot shows the total potential U_{pi} between a fullerene and a single BER bead at distance R . The dashed lines represent the implicit model we use in this study. For comparison the potential curves for explicit CG bead models of C_{60} and C_{540} are also shown. The explicit potentials were generated by sampling the different rotational orientations of the fullerene according to their Boltzmann weight. As seen in Fig. (4) the potentials for the implicit and explicit fullerene models are in excellent agreement.

Among the reasons motivating the use of an implicit mean field model are the novel techniques which yield thermodynamic information which are not possible with an explicit bead model. For example, the method we use to evaluate the solvation free energies relies on the ability to calculate the force acting on the fullerene radius. This is only available in the mean field model where the

¹ The BER bead maps to 1.5 aromatic carbon atoms. Hence an atomic site density of 0.39 \AA^{-2} translates to a coarse grained site density of 0.26 \AA^{-2} .

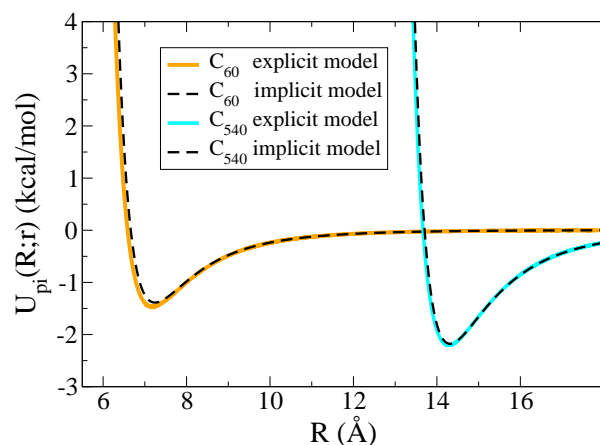


Fig. (4). The potential energy curves for the interaction of a fullerene with a bead (of BER type). The solid lines are for an explicit CG bead fullerene model while the dashed lines are from the implicit model developed in this study. The mean field model is seen to be an excellent approximation across a wide range of fullerene sizes. Even the slight deviation in potential between the explicit coarse grained and continuum model of C_{60} may be attributed to the constant value of ρ_s we use for all sizes of fullerenes, while in actuality the site densities of fullerenes (ρ_s) vary slightly with their size.

fullerene-soft matter bead interaction potential energies are parametrically dependent on the fullerene radius. Furthermore, the analytical form of the potentials (see Eq. 3) give valuable insight into how the hollow nature of the fullerene impacts its behavior.

Comparison of the Hollow and Filled Sphere Potentials

The behavior of solid particles is determined by their interaction potentials with the environment. These potentials depend, in part, on the structure of the particle. To fully understand the behavior of fullerenes it is important to conceptualize the difference between a hollow and a filled spherical particle, particularly since most colloids theories assume a filled geometry.

The use of the implicit mean field model allows us to analytically evaluate the potential energy expressions for the fullerenes represented by a continuum hollow sphere (see Eq. 3). Let us name this potential $U_{pi}^{hs}(R;r)$. The same approach can be used for a filled sphere as described in our previous work [26]; the important change being the integral to obtain the net interaction (U_{pi}^{fs}) involves a third dimension for the particle volume.

For a given radius the filled sphere encompasses a greater number of interaction sites leading to a deeper potential well for the interaction with a soft matter bead. The particle-liquid interaction potential is plotted in Fig. (5) for both a hollow sphere $U_{pi}^{hs}(R;r)$ and a filled sphere $U_{pi}^{fs}(R;r)$. For $U_{pi}^{hs}(R;r)$ we have used the parameters for C_{540} ($r = 10.55 \text{ \AA}$, $\rho_s = 0.26 \text{ \AA}^{-2}$, $\epsilon = 0.1750 \text{ kcal mol}^{-1}$, $\sigma = 3.800 \text{ \AA}$). For the filled sphere potential we have used the same parameters; however, the surface site density ρ_s must be changed to a volume site density ρ_v , the value of which is chosen to correspond to bulk graphite ($\rho_v = 0.07533 \text{ \AA}^{-3}$).

Fig. (5) also shows $U_{pi}^{hs}(R;r)$ scaled by a factor $C = 5.35$ such that the value at the minima of $U_{pi}^{fs}(R;r)$ and $U_{pi}^{hs}(R;r)$ are equal. This plot shows that the onset of the repulsion occurs at larger R values for the hollow sphere. The repulsion is caused by the overlap of electron clouds (Pauli exclusion), which is directly felt by any

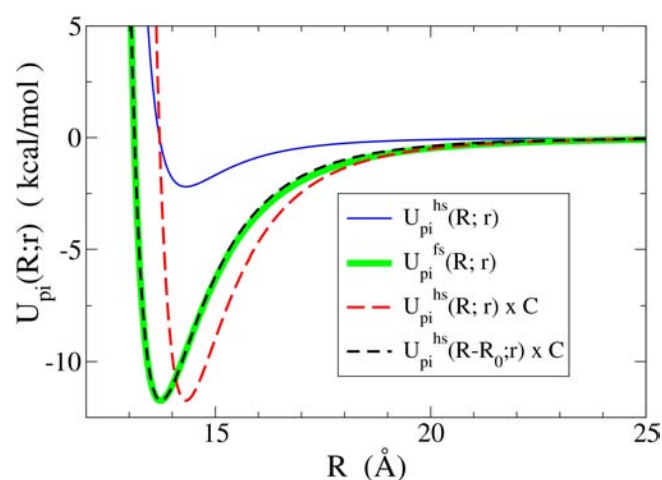


Fig. (5). The comparison of the particle-liquid interaction potential for a hollow sphere $U_{pi}^{hs}(R;r)$ (thin solid curve) and a filled sphere $U_{pi}^{fs}(R;r)$ (thick solid curve) interacting with a BER type bead. The hollow sphere potential corresponds to C_{540} while the solid potential corresponds to a graphitic particle of the same radius. The light dashed line ($U_{pi}^{hs}(R;r) \times C$) shows the hollow sphere potential scaled to match the filled sphere potential minimum, and the dark dashed line ($U_{pi}^{hs}(R-R_0;r) \times C$) shows the scaled and offset hollow sphere potential.

atom approaching the hollow spherical particle. This is due to a finite interaction site density precisely at the sphere surface in the case of the hollow sphere, which is not the case for the filled sphere where the interaction sites are uniformly distributed over the particle volume.

Other than the differences in the relative magnitude of interactions between a filled particle and a hollow particle, the decay of the potentials with separation shows a similar form. To illustrate this graphically $U_{pi}^{hs}(R;r) \times C$ is offset by $R_0 = 0.58 \text{ \AA}$ which superimposes the hollow sphere potential with that of the filled sphere.

To conclude this section we note that the physical behavior of fullerenes in a fluid environment results from two primary factors. The first is the nature of the surface atoms presented to the environment. This is captured through our use of the BER building block. The second is the hollow shell geometry of the fullerenes. This is captured through our continuum model for the hollow sphere.

Fullerenes in a Lipid Bilayer Environment

The behavior of fullerenes in a DOPC lipid bilayer is related to the chemistry of the lipids and the properties of the membrane. The phosphatidylcholines (PCs) are a major component of biological membranes, and in particular DOPC (dioleoylphosphatidylcholine) is the most abundant PC in living organisms [33]. In general lipids are composed of two hydrocarbon chains pendant from a polar glycine head group; this amphiphilic structure facilitates spontaneous self assembly in water. The bilayer membrane is such an assembly, where the lipids align in two parallel sheets with their polar heads directed outwards into the water phase and their non-polar tails creating a hydrophobic region in between. This bilayer structure forms a physical barrier for the diffusion of hydrophilic solutes, giving it biological significance.

Simulations of fullerenes in DOPC bilayers were carried out by growing the size of the fullerene from zero to 11 \AA (see Methods

section) separately in water and in the DOPC bilayer membrane. Fig. (6) shows representative snapshots of some of the sizes of particles simulated in DOPC.

When fullerenes are introduced into a lipid bilayer, they are seen to favor localizing in the non-polar environment of the hydrocarbon chains, but with a size dependent distribution of their position with respect to the bilayer center. Fig. (7) plots this distribution as a function of particle size. The overall trend within the physically significant region ($r \geq 3 \text{ \AA}$) is that larger fullerenes are found closer to the center of the membrane. At very small radii the model loses physical significance and these sizes of fullerenes are only included in the study in order to calculate the solvation free energy.

Generally the fullerenes prefer localizing in the center of the acyl chains of one leaflet, while avoiding the center of the bilayer (methyl trough) because this would incur an entropic penalty from subduing the conformational freedom of the lipid tails. However, the barrier for passing through the methyl trough is low enough that all sizes of fullerenes move between the two leaflets over the course of 50 ns simulations. With increasing size the fullerenes would disrupt the structure of the lipid head group-water interface if they were situated at the center of the acyl chains and hence are instead pushed towards the center of the bilayer. Smaller sizes of fullerenes therefore result in broad distributions which are peaked closer to the head groups while larger particles show narrow position distributions which peak closer to the center of the bilayer membrane (see Fig. 7).

Solvation Free Energies

The solvation free energy is defined as the free energy required to transfer an object from an ideal gas phase reference state into its solvated environment. With water as the solvent, this is the hydration free energy, G_{wat} . Intimately tied to this concept is the thermodynamic definition for hydrophobicity/hydrophilicity where an object with $G_{wat} < 0$ is considered to be hydrophilic.

Conventionally the free energy of solvation can be found through molecular simulation by displacing the object from one environment to the other in a system containing the appropriate interface. Constrained molecular dynamics or steered molecular dynamics are common techniques used to enact this displacement [34]. However, in these approaches a series of simulations is needed to obtain the solvation free energy of a specific fullerene.

Instead, in this study we use a novel method for evaluating the solvation free energy by 'growing' fullerenes in solvent. As described in the Methods section the free energy of growing a particle in solvent (see Eq. 4) can be found through the mean force acting on the particle radius for a series of increasing particle sizes. The primary advantage of this approach is that through a single

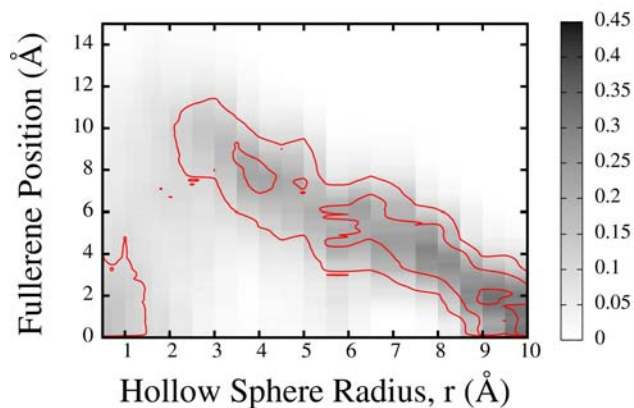


Fig. (7). The position distribution of fullerenes in the DOPC bilayer membrane as a function of particle size. The darker areas show regions of higher probability. The fullerene positions are measured relative to their distance from the bilayer central plane. The smaller radius particles tend to have broader distributions while they have a higher probability of being found close to the head groups of the lipids. As the particle size becomes larger the particles tend to move to the center of the bilayer and have narrower distributions.

series of simulations we can obtain the solvation free energies for fullerenes of many different sizes. This scheme was carried out for fullerenes in water and in a DOPC bilayer membrane environment, and the resulting free energy plots are given in Fig. (8).

The solvation free energy curves are roughly quadratic as would be expected since the particle-solvent surface area increases as the square of the particle radius. It is interesting to note that solvation in both water and the lipid membrane is favorable ($G_{solv} < 0$). Although this is expected for fullerenes in the hydrophobic interior of the lipid membrane, the result that fullerenes are hydrophilic is somewhat surprising. However, it has recently been suggested that even long *n*-alkanes are hydrophilic [35], and Athawale *et al.* have pointed out that the commonly used all-atom graphite-water force fields all predict $G_{wat} < 0$ for spherical fullerenes [36]. It should be noted that although the hydration free energy of fullerenes is negative this is not indicative of their solubility in water, because the fullerene-fullerene interaction also plays a role in determining solubility.

From the absolute solvation free energies, the transfer free energy of the fullerene from lipid to water is found by using a thermodynamic cycle (see Fig. 9).

Fig. (10) shows the variation of transfer free energy as a function of fullerene size. Superimposed on this figure are the

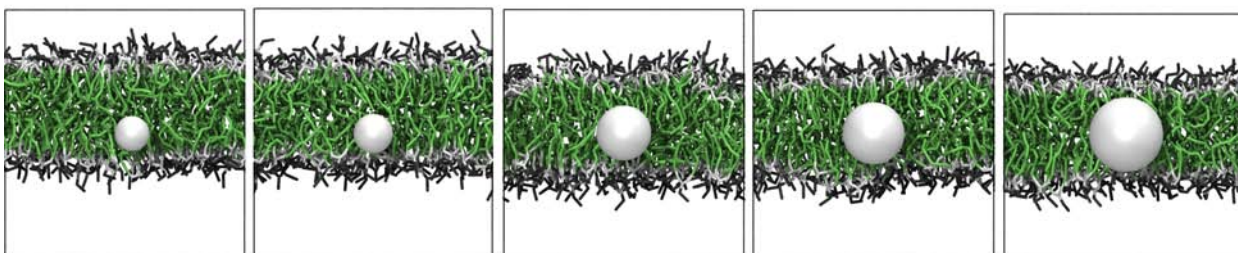


Fig. (6). Different sized fullerenes in DOPC lipid bilayers. From left to right, the particle size corresponds to C_{60} , C_{80} , C_{240} , C_{320} and C_{540} . The color scheme is similar to Fig. (2), while the fullerenes are shown in front of the lipids for clarity. The distribution of the fullerene position changes as a function of particle size as shown in Fig. (7).

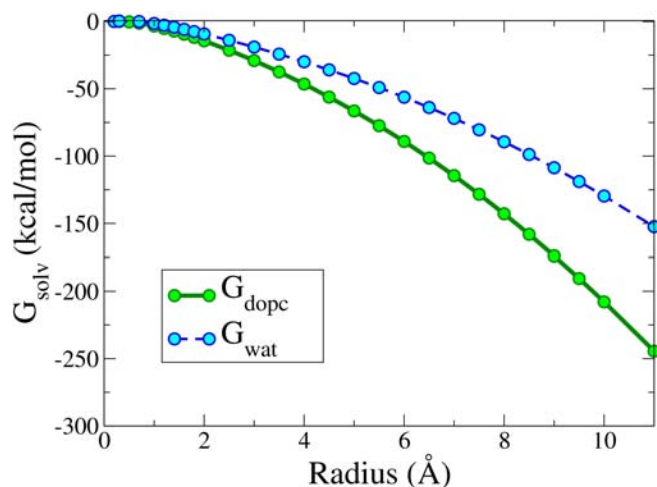


Fig. (8). The absolute solvation free energies of fullerenes in a DOPC lipid bilayer (G_{dopc} , shown in the solid line) and water (G_{wat} , shown in the dashed line) as a function of fullerene size.

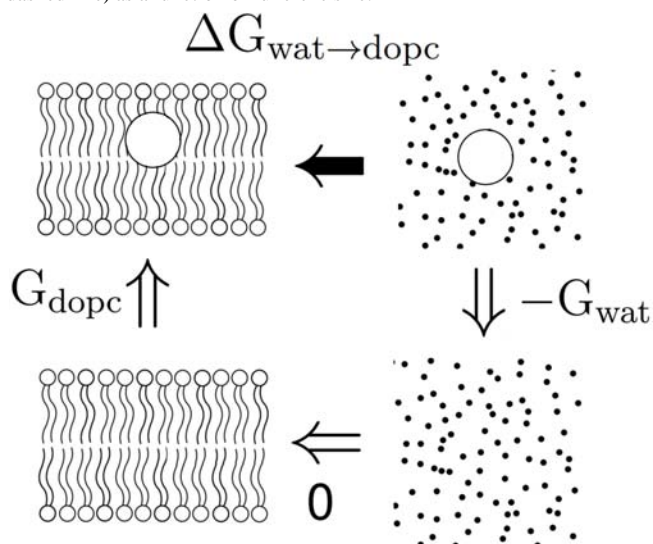


Fig. (9). The thermodynamic cycle used to obtain the transfer free energy of a fullerene from water to DOPC. The transfer free energy (black arrow) can be obtained by the following route: (1) shrinking the fullerene in water, which is the negative of the solvation free energy G_{wat} , (2) transferring the particle of zero radius into DOPC which incurs no free energy cost, and (3) growing the fullerene back in the lipid bilayer, which is the solvation free energy G_{dopc} .

transfer free energy values for explicit fullerene models taken from the literature [14]. Both all-atom and CG models are used for comparison, and show qualitative agreement with the mean field model. However, different temperature and barostatting conditions were used in these MD studies so quantitative agreement cannot be expected.

Furthermore, it has been reported from both all-atom and CG explicit model studies that there is no free energy barrier for the entry of a fullerene molecule into the lipid bilayer membrane from the water phase [14]. As a result there exists a direct correlation between the transfer free energy and the partitioning of different sizes of fullerenes in the membrane through passive diffusion. Therefore this method may be useful in eventually characterizing and predicting the partitioning of fullerenes in biological membranes, particularly in view of the range of sizes and surface chemistry these molecules have.

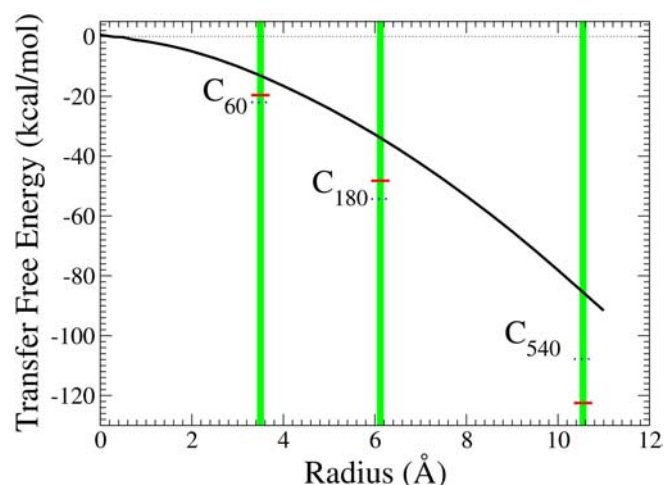


Fig. (10). The relative water to DOPC bilayer transfer free energies are plotted as a function of fullerene size. Also shown are the transfer free energies for explicit models of C_{60} , C_{180} and C_{540} taken from the literature. The dashed horizontal lines represent the all-atom data while the solid lines represent CG data. The data taken from the literature was obtained under different temperature and pressure conditions.

CONCLUSIONS

In summary we have proposed and implemented an implicit mean field model of fullerenes in lipid bilayer systems. Here the fullerene is considered a hollow sphere of uniform interaction site density, which accurately captures both its surface characteristics and geometry. This model is compatible with state of the art coarse-grained molecular dynamics force fields and can be readily used in simulations of soft matter systems such as lipid bilayers, as exemplified by the qualitative agreement we observe with recently published explicit models of C_{60} , C_{180} and C_{540} . The continuum model used to represent the fullerenes results in a force field in which the fullerene-soft matter interaction energies are parametrically dependent on the fullerene radius. This dependence is exploited using our novel approach [30] to efficiently evaluate the fullerene solvation free energy in several environments. Using a thermodynamic cycle we are then able to evaluate the water to lipid transfer free energies of fullerenes of different sizes, using a single series of simulations. The results of this study give us an improved understanding of the size dependent solubility and potential effects of fullerenes on biological systems.

Although this article has focused on individual fullerenes in lipid membranes, the understanding of fullerene-fullerene interactions, and particularly aggregation behavior, is thought to be an important aspect of their potential toxicity. The systems studied here can easily be extended to include more than one fullerene particle and this would be an interesting avenue of future research.

ACKNOWLEDGEMENTS

We gratefully acknowledge the financial support of the SRC/SEMATECH Engineering Research Center for Environmentally Benign Semiconductor Manufacturing.

REFERENCES

- [1] Gil, P. R.; Oberdorster, G.; Elder, A.; Puentes, V.; Parak, W. J. Correlating physico-chemical with toxicological properties of nanoparticles: The present and the future. *ACS Nano*, **2010**, *4*, 5527-5531.
- [2] Yan, L.; Zhao, F.; Li, S.; Hu, Z.; Zhao, Y. Low-toxic and safe nanomaterials by surface-chemical design, carbon nanotubes, fullerenes, metallofullerenes, and graphenes. *Nanoscale*, **2010**, *3*, 362-382.
- [3] Delgado, J. L.; Bouit, P.-A.; Filippone, S.; Herranz, M. A.; Martin, N. Organic photovoltaics: A chemical approach. *Chem. Commun.*, **2010**, *46*, 4853-4865.

- [4] Farro, L.; Mihaly, L. Electronic properties of doped fullerenes. *Rep. Prog. Phys.*, **2001**, *64*, 649-699.
- [5] Yifeng, E.; Bai, L.; Fan, L.; Han, M.; Zhang, X.; Yang, S. Electrochemically generated fluorescent fullerene[60] nanoparticles as a new and viable bioimaging platform. *J. Mater. Chem.*, **2011**, *21*, 819-823.
- [6] Liu, J.-H.; Cao, L.; Luo, P. G.; Yang, S.-T.; Lu, F.; Wang, H.; Mezzani, M. J.; Haque, S. A.; Liu, Y.; Lacher, S.; Sun, Y.-P. Fullerene-conjugated doxorubicin in cells. *Appl. Mater. Interf.*, **2010**, *2*, 1384-1389.
- [7] Aschberger, K.; Johnston, H. J.; Stone, V.; Aitken, R. J.; Tran, C. L.; Hankin, S. M.; Peters, S. A.; Christensen, F. M. Review of fullerene toxicity and exposure - Appraisal of a human health risk assessment, based on open literature. *Regul. Toxicol. Pharmacol.*, **2010**, *58*, 455-473.
- [8] Johnston, H. J.; Hutchinson, G. R.; Christensen, F. M.; Aschberger, K.; Stone, V. The biological mechanisms and physicochemical characteristics responsible for driving fullerene toxicity. *Toxicol. Sci.*, **2010**, *114*, 162-182.
- [9] Nielsen, G. D.; Roursgaard, M.; Jensen, K. A.; Poulsen, S. S.; Larsen, S. T. *In vivo* biology and toxicology of fullerenes and their derivatives. *Basic Clin. Pharmacol. Toxicol.*, **2008**, *103*, 197-208.
- [10] Rouse, J. G.; Yang, J.; Ryman-Rasmussen, J. P.; Barron, A. R.; Monteiro-Riviere, N. A. Effects of mechanical flexion on the penetration of fullerene amino acid-derivatized peptide nanoparticles through skin. *Nano Lett.*, **2007**, *7*, 155-160.
- [11] Yamawaki, H.; Iwai, N. Cytotoxicity of water-soluble fullerene in vascular endothelial cells. *Am. J. Physiol. Cell. Physiol.*, **2006**, *290*, C1495-C1502.
- [12] Wong-Ekkabut, J.; Baoukina, S.; Triampo, W.; Tang, I.-M.; Tieleman, D. P.; Monticelli, L. Computer simulation study of fullerene translocation through lipid membranes. *Nat. Nano*, **2008**, *3*, 363-368.
- [13] Monticelli, L.; Salonen, E.; Ke, P. C.; Vattulainen, I. Effects of carbon nanoparticles on lipid membranes: A molecular simulation perspective. *Soft Matter*, **2009**, *5*, 4433-4445.
- [14] Jusufi, A.; DeVane, R. H.; Shinoda, W.; Klein, M. L. Nanoscale carbon particles and the stability of lipid bilayers. *Soft Matter*, **2011**, *7*, 1139-1146.
- [15] Bedrov, D.; Smith, G. D.; Davande, H.; Li, L. Passive transport of C₆₀ fullerenes through a lipid membrane: A molecular dynamics simulation study. *J. Phys. Chem. B*, **2008**, *112*, 2078-2084.
- [16] Qiao, R.; Roberts, A. P.; Mount, A. S.; Klaine, S. J.; Ke, P. C. Translocation of C₆₀ and its derivatives across a lipid bilayer. *Nano Lett.*, **2007**, *7*, 614-619.
- [17] D'Rozario, R. G. D.; Wee, C. L.; Wallace, E. J.; Sansom, M. S. P. The interaction of C₆₀ and its derivatives with a lipid bilayer via molecular dynamics simulations. *Nanotechnology*, **2009**, *20*, 115102.
- [18] Mutlu, G. M.; Budinger, G. R. S.; Green, A. A.; Urlich, D.; Soberanes, S.; Chiarella, S. E.; Alheid, G. F.; McCrimmon, D. R.; Szeifer, I.; Hersam, M. C. Biocompatible nanoscale dispersion of single-walled carbon nanotubes minimizes *in vivo* pulmonary toxicity. *Nano Lett.*, **2010**, *10*, 1664-1670.
- [19] Hamaker, H. C. The London - van der Waals attraction between spherical particles. *Physica (Amsterdam)*, **1937**, *4*, 1058-1072.
- [20] Henderson, D.; Plischke, M. Calculation of the density profile of a system of hard spheres near a hard wall using the Henderson-Plischke and related approximations. *J. Chem. Sci.*, **1986**, *97*, 297-305.
- [21] Girifalco, L. A. Molecular properties of C₆₀ in the gas and solid phases. *J. Phys. Chem.*, **1992**, *96*, 858-861.
- [22] Shinoda, W.; DeVane, R.; Klein, M. L. Coarse-grained molecular modeling of non-ionic surfactant self-assembly. *Soft Matter*, **2008**, *4*, 2454-2462.
- [23] Shinoda, W.; DeVane, R.; Klein, M. L. Multi-property fitting and parameterization of a coarse grained model for aqueous surfactants. *Mol. Simul.*, **2006**, *33*, 27-26.
- [24] Shinoda, W.; DeVane, R.; Klein, M. L. Zwitterionic lipid assemblies: Molecular dynamics studies of monolayers, bilayers, and vesicles using a new coarse grain force field. *J. Phys. Chem. B*, **2010**, *114*, 6836-6849.
- [25] Kalescky, R. J. B.; Shinoda, W.; Moore, P. B.; Nielsen, S. O. Area per ligand as a function of nanoparticle radius: A theoretical and computer simulation approach. *Langmuir*, **2009**, *25*, 1352-1359.
- [26] Chiu, C.-c.; Moore, P. B.; Shinoda, W.; Nielsen, S. O. Size-dependent hydrophobic to hydrophilic transition for nanoparticles: A molecular dynamics study. *J. Chem. Phys.*, **2009**, *131*, 244706.
- [27] Plimpton, S. Fast parallel algorithms for short-range molecular dynamics. *J. Comput. Phys.*, **1995**, *117*, 1-19.
- [28] Hoover, W. G. Canonical dynamics: Equilibrium phase-space distributions. *Phys. Rev. A*, **1985**, *31*, 1695-1697.
- [29] Tuckerman, M. E.; Berne, B. J.; Martyna, G. J. Molecular dynamics algorithm for multiple time scales: Systems with long range forces. *J. Chem. Phys.*, **1991**, *94*, 6811-6815.
- [30] Chiu, C.-c.; Ranatunga, R. J. K. U.; Flores, D. T.; Perez, D. V.; Moore, P. B.; Shinoda, W.; Nielsen, S. O. A mean field approach for computing solid-liquid surface tension for nanoscale interfaces. *J. Chem. Phys.*, **2010**, *132*, 054706.
- [31] DeVane, R.; Klein, M. L.; Chiu, C.-c.; Nielsen, S. O.; Shinoda, W.; Moore, P. B. Coarse-grained potential models for phenyl-based molecules: I. Parameterization using experimental data. *J. Phys. Chem. B*, **2010**, *114*, 6386-6393.
- [32] DeVane, R.; Jusufi, A.; Shinoda, W.; Chiu, C.-c.; Nielsen, S. O.; Moore, P. B.; Klein, M. L. Parameterization and application of a coarse grained force field for benzene/fullerene interaction with lipids. *J. Phys. Chem. B*, **2010**, *114*, 16364-16372.
- [33] Garrett, R. H.; Grisham, C. M. *Biochemistry*; Thomson Brooks/Cole, **2007**.
- [34] *Free Energy Calculations*; Chipot, C., Pohorille, A., Eds.; Springer: Berlin, **2007**.
- [35] Underwood, R.; Tomlinson-Phillips, J.; Ben-Amotz, D. Are long-chain alkanes hydrophilic? *J. Phys. Chem. B*, **2010**, *114*, 8646-8651.
- [36] Athawale, M. V.; Jamadagni, S. N.; Garde, S. How hydrophobic hydration responds to solute size and attractions: Theory and simulations. *J. Chem. Phys.*, **2009**, *131*, 115102.